

Mechanically-robust structural lithium-sulfur battery with high energy density[☆]

Wenlong Huang^{a,b,1}, Peiyu Wang^{a,1}, Xiangbiao Liao^c, Yijun Chen^a, James Borovilas^a, Tianwei Jin^a, Aijun Li^a, Qian Cheng^a, Yifan Zhang^a, Haowei Zhai^a, Adrain Chitu^a, Zhongqiang Shan^b, Yuan Yang^{a,*}

^a Program of Materials Science and Engineering, Department of Applied Physics and Applied Mathematics, Columbia University, New York, NY 10027, United States

^b School of Chemical Engineering and Technology, Tianjin University, Tianjin 300350, China

^c Earth Engineering Center, Center for Advanced Materials for Energy and Environment, Department of Earth and Environmental Engineering, Columbia University, New York, NY 10027, United States

ARTICLE INFO

Keywords:

Structural energy storage
electrodeposition-like electrode
mechanically robustness
lithium-sulfur battery

ABSTRACT

The development of structural batteries has been obstructed by the intrinsically low mechanical strength of battery materials inside. Here, we propose a multifunctional structural battery platform by deploying electrodeposition-like reactions to prepare for conformally-coated electrodes, together with carbon fabrics as the skeleton to endow them with mechanical robustness. As a proof of concept, the Li/S battery system based on the electrodeposition-like mechanism was introduced into the structural batteries for the first time. The Young's modulus of optimized sulfur and lithium electrodes reach 9.2 ± 1.2 GPa and 4.5 ± 0.6 GPa, respectively, 5–20 times higher than conventional electrodes. Additionally, a thermally stable composite separator combining boron nitride nanofiller with PVdF polymer (BN/PVdF) is rationally designed, which possesses high compressive strength over 180 MPa. The structural cell integrated with these structural components delivered an excellent lifespan under compression up to 20 MPa for 20 cycles at 0.2 C. Moreover, the structural Li/S cell in pouch configuration displays better resistance to mechanical deformation when compared to the regular Li/S cell. This work provides valuable insight into structural batteries with high energy density.

1. Introduction

Lightweighting is critical for enhancing the energy efficiency of electrified-transportation, such as aircraft and electrical vehicles [1,2]. The development of multifunctional materials to integrate different functionalities into a single component is an attractive concept in lightweighting [3,4]. For example, the structural supporting components can be used for energy production (e.g. solar cells or kinetic energy harvesting) [5,6] or storage (e.g. supercapacitors or batteries) [7–9] so as to reduce the overall weight. Structural energy storage is a kind of functional energy storage devices that can withstand mechanical stress [10]. The concept centers on combining the mechanical performance of composites with structural components in batteries or supercapacitors [9]. This is closely related to the pursuit of lightweight cube satellites and aircraft, thus maximizing the propulsion of power sources and resistance to the damage from high velocity impact [11,12]. To combine energy storage and structural functionality together, the

structural battery must have robust mechanical properties to adapt to various kinds of deformation (i.e., compression, stretch, etc.), while maintaining excellent electrochemical performance, including but not limited to the rate capability, cycling stability with reasonable cycle life. Moreover, these batteries should function safely under mechanical deformation during operation.

In recent years, several groups have conducted pioneering works on structural supercapacitors by using carbon fiber or graphene-based materials as the mechanical support and active materials [10,13–16]. Reasonable electrochemical performance with improved mechanical properties has been demonstrated, but the specific energy is typically lower than 1.0 Wh kg^{-1} [17,18]. The same strategy has been applied to structural lithium-ion batteries but limited success has been achieved [17,19]. On the one hand, due to the particle properties and the insertion/extraction-type reaction mechanism, it is easy for electrode materials to delaminate from planar current collectors (Fig. 1a, Supplementary Video S1) or lose intact contact with 3D conductive matrix, e.g. carbon fiber fabrics (Fig. 1b, Supplementary Video S1), which

[☆] The authors declare no conflict of interest.

* Corresponding author.

E-mail address: yy2664@columbia.edu (Y. Yang).

¹ W. Huang and P. Wang contributed equally to this work.

not only increases the electronic resistance but also reduces the mechanical strength of the whole battery [17,20,21]. On the other hand, if lithium ions intercalate into carbon fibers (e.g. in Li-ion anodes), the mechanical strength of carbon fibers will be significantly compromised, therefore failing to maintain long-lasting mechanical strength for structural lithium-ion batteries [22,23].

Different from the particle-based electrodes with its active materials attached to the substrates by additional binder, electrodeposition-like electrode means active materials are transformed from the electrolyte to the conductive substrate similar to electrochemical deposition, therefore reducing the risk of the contact deterioration or the delamination of active materials from the substrate with external mechanical load. In other words, electrodes utilizing electrodeposition-like mechanism to coat active materials conformally on mechanical supports, along with some beneficial functional groups to enhance their interaction can provide more possibilities beyond lithium-ion batteries [24,25], but these advantages have yet been considered in the field of structural batteries. As a proof of concept, Li/S battery system based on the electrodeposition-like mechanism was introduced into the structural batteries, where polysulfide catholyte and molten lithium metal are adopted as alternatives to prepare for the cathode and anode, respectively, together with carbon fabric skeleton to endow them with mechanical robustness. The design idea is different from conventional thinking in previous structural batteries. The novelty highlights in utilizing the conformally-coated strategies to design structural electrodes that effectively avoids the tricky problems in structural lithium-ion batteries, e.g. high ohm resistance caused by loose contact and weak resistance to mechanical deformation.

As far as we know, it is the first attempt to introduce the lithium-sulfur system into structural batteries. Specifically, carbon fabrics (T300, 3 K) is combined with 1 M polysulfide catholyte as the cathode, enabling sulfur and $\text{Li}_2\text{S}_2/\text{Li}_2\text{S}$ to be conformally electrodeposited onto the carbon fibers during the charge/discharge process, thus avoiding poor contact between solid particles and carbon fibers (Fig. 1b). On the anode side, molten lithium is infiltrated into the carbon fiber matrix. Although the unavoidable Li intercalation reduces the mechanical properties of carbon fibers, the excessive lithium metal can act as a glue to

bind lithiated carbon fibers together, thereby enhancing the mechanical strength of the anode. The reinforced cathode and anode have Young's modulus of 9.2 ± 1.2 GPa and 4.5 ± 0.6 GPa, respectively, and exhibit the corresponding ultimate tensile strength (UTS) of 214 ± 16 MPa and 53 ± 7 MPa, which are all 1–2 orders of magnitude higher than those of conventional particle-based electrodes.

In order to achieve a synergistic lifespan for the whole battery under mechanical load, we also developed a new BN/PVdF separator as the structural component specifically for the structural Li/S battery above. The introduction of the high-modulus inorganic filler enhances the compressive strength of the separator effectively. Furthermore, the thermally-stable BN/PVdF film can be used with liquid electrolyte safely, which alleviates the poor lithium ion conductivity compared to conventional structural batteries [13,26,27]. Owing to the introduction of BN nanosheets, the as-fabricated BN/PVdF composite separator possesses UTS of 13.1 ± 1.2 MPa and isotropic Young's modulus of 1.2 ± 0.2 GPa, significantly superior to that of the regular PE separator (Celgard 2325) in the transverse direction (8.0 ± 0.6 MPa and 0.26 ± 0.05 GPa). In combination of the well-designed structural electrodes with the BN/PVdF separator, the Li/S cell shows good electrochemical performance with an initial discharge capacity of 1266 mAh g^{-1} and capacity retention of 81% after 200 cycles at 0.2 C. Under 20 MPa compression, the structural Li/S cell delivers an excellent synergistic lifespan up to 20 cycles at 0.2 C and possesses better resistance to mechanical deformation when compared to the regular Li/S cell in their pouch configurations. These results demonstrate the feasibility of this new strategy to improve the mechanical strength of structural batteries with high energy density.

2. Results and discussion

In our design, the cathode is made of commercial T300 CF in combination with 2.0 M Li_2S_8 (the concentration is based on [S]) in 1,3-dioxolane/1,2-dimethoxyethane (DOL/DME) as the structural skeleton. The pristine CF consists of horizontal and vertical carbon bundles where the diameter of filament is $\sim 7 \mu\text{m}$ (inset in Fig. S2a), which possesses UTS of 232 ± 8 MPa and Young's modulus of 22 ± 1.6 GPa (Fig. 2c and

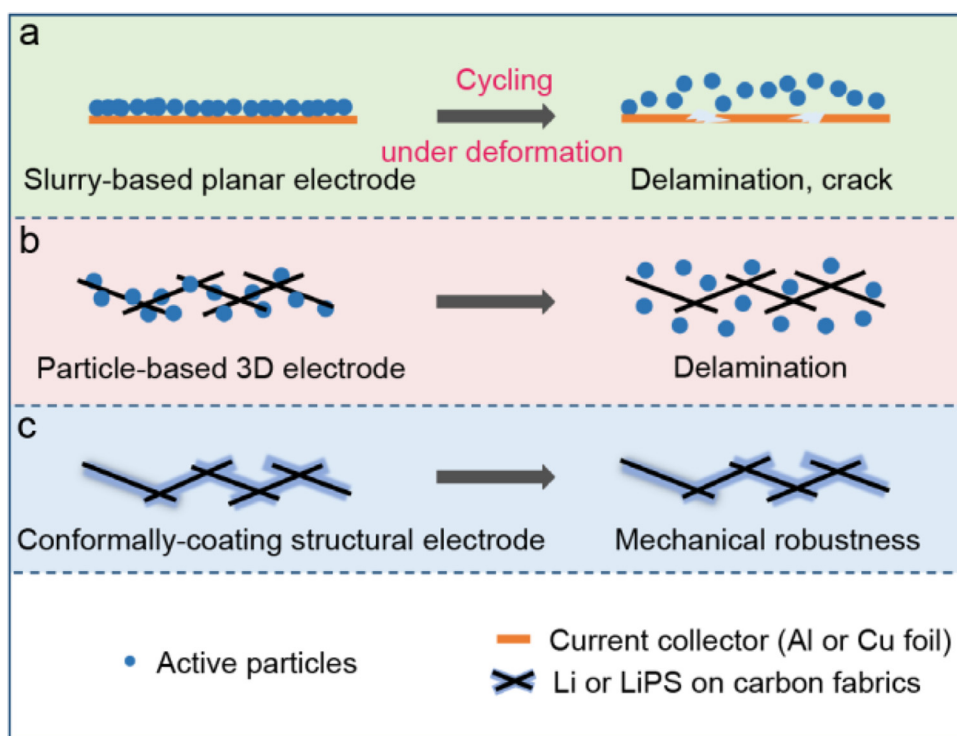


Fig. 1. The design principle of electrodeposition-like electrodes for structural energy storage. (a) An illustration of the intrinsically low mechanical strength of particle-based planar electrodes, suffering from the delamination of active materials or crack of current collectors (Al or Cu foil) during cycling under deformation. (b) An illustration of the delamination of active materials from carbon fibers during cycling under deformation, due to the weak solid-solid interactions. (c) An illustration of the enhanced strength via electrodeposition-like reaction on structural skeleton. The detailed information can be obtained in Supplementary Video S1 and Fig. S1.

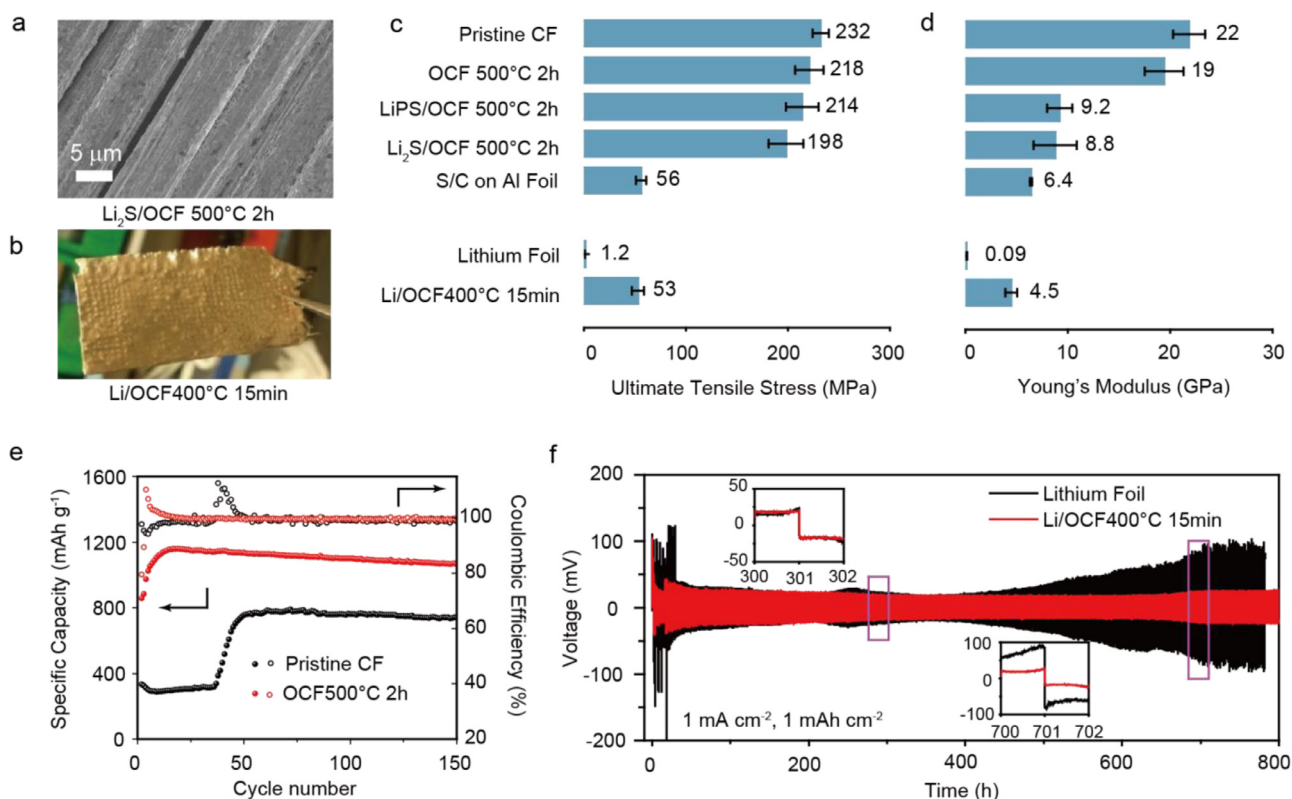


Fig. 2. (a) The surface morphology of OCF after depositing of Li₂S. (b) Digital image of a piece of OCF after infiltrating the molten lithium. (c) The UTS and (d) Young's modulus of carbon fiber-reinforced electrodes in comparison to conventional particle-based electrodes. (e) The cycling performance of the polysulfide cathode with pristine CF (black curve) and OCF 500 °C 2 h (red curve). (f) The cycling stability of Li/Li symmetric cells with conventional Li foil (black) and Li/OCF composite in b. The current and the deposited capacity are 1.0 mA cm⁻² and 1.0 mAh cm⁻², respectively. The inset shows the voltage profile at the 150th and 350th cycle.

2d). However, since the polymer-based sizing agent on the fiber surface impedes electron transport (Fig. S2b-2d), the initial discharge capacity of the cathode is only ~ 300 mAh g⁻¹, as illustrated in Fig. 2e. Upon cycling, the discharge capacity gradually increases to ~ 800 mAh g⁻¹, which might arise from the swelling and even dissolution of the sizing agent in the electrolyte. Despite this, the capacity is relatively lower than the previously reported values [28–30].

To enhance the electrochemical performance of the structural cathode, the pristine CF is heated in air to remove the sizing agent. These heated samples are denoted as oxidized carbon fabric (OCF). The properties of pristine CF treated at different temperatures and time are also studied (Fig. S3a-S3b), and 500 °C for 2 h is the optimal condition to obtain the balance between the mechanical and electrochemical properties of the corresponding structural cathode. The detailed mechanism for the heating treatment is further analyzed in the supporting information, which is related to the proportion of the C-C/C=O groups on the CF surface (Fig. S3d and Table S1). Although OCF shows slightly compromised mechanical strength, namely UTS of 218 ± 14 MPa after heating, 214 ± 16 MPa after soaking with the polysulfide catholyte and 198 ± 17 MPa after electrodepositing Li₂S, however, such mechanical properties are still four times higher than conventional particle-based cathodes on Al foil (56 ± 5 MPa, Fig. S4d). The Young's modulus shows the same trend with the value of 19 ± 1.7 GPa after heating, 9.2 ± 1.2 after soaking with 1 M polysulfide catholyte and 8.8 ± 2.1 GPa after electrodepositing Li₂S, much higher than the conventional sulfur cathode (6.4 ± 0.1 GPa). More details can be found in Fig. S4a-S4d. Despite this, the electrochemical performance of OCF-reinforced sulfur cathode was dramatically improved after the thermal treatment. The initial capacity reaches 1159 mAh g⁻¹ and the capacity retention is 91.9% after 150 cycles at 0.2 C (Fig. 2e). The excellent electrochemical reversibility

can be attributed to uniform deposition and improved interactions of polysulfide species with carbon fibers.

On the other hand, lithium metal is infiltrated into OCF to enhance the mechanical strength of anode. It should be noted that the sizing agent on CF is removed by pre-heating at 400 °C in air for 15 min to promote its lithophilic property. (Supplementary Video S2 and Table S2). Once thermally annealed, the oxygen-containing functional groups on the carbon fiber surface enable lithium metal to infiltrate into the OCF matrix easily [31,32]. The result shown in Fig. S5a-S5c indicates that the OCF skeleton greatly strengthened the lithium anode. Specifically, the UTS improves from 1.2 ± 0.2 MPa (pure lithium strip) to 53 ± 7 MPa (Li/OCF 400 °C 15 min) while the Young's modulus increases dramatically from 0.09 ± 0.05 GPa to 4.5 ± 0.6 GPa, respectively (Fig. 2c and 2d). The significant enhancement originates from the load transfer from lithium metal to the interconnected OCF network, similar to the results in a previous report [33].

The OCF-reinforced lithium anode with a thickness of ~ 250 μm also shows improved electrochemical performance. As shown in Fig. 2f, the Li/Li symmetric cell with Li/OCF electrodes exhibits a stable voltage profile and a small overpotential of 20 mV over 800 h at the current density of 1.0 mA cm⁻². In comparison, the cell using lithium foil electrodes shows poor cycling stability with increasing overpotential during repeated stripping/plating process. This improved cycling performance stems from the larger surface area in the Li/OCF composite electrode [32]. Although Li fills most regions inside carbon fibers, there are always voids left that accommodate for the deposited lithium metal. Therefore, even at a higher current density of 3.0 mA cm⁻², the stripping/plating stability for Li/OCF electrodes is much better than that of pure lithium metal anodes (Fig. S5d). From the morphologies of the anodes after cycling, the surface of pure lithium foil presents a porous structure while

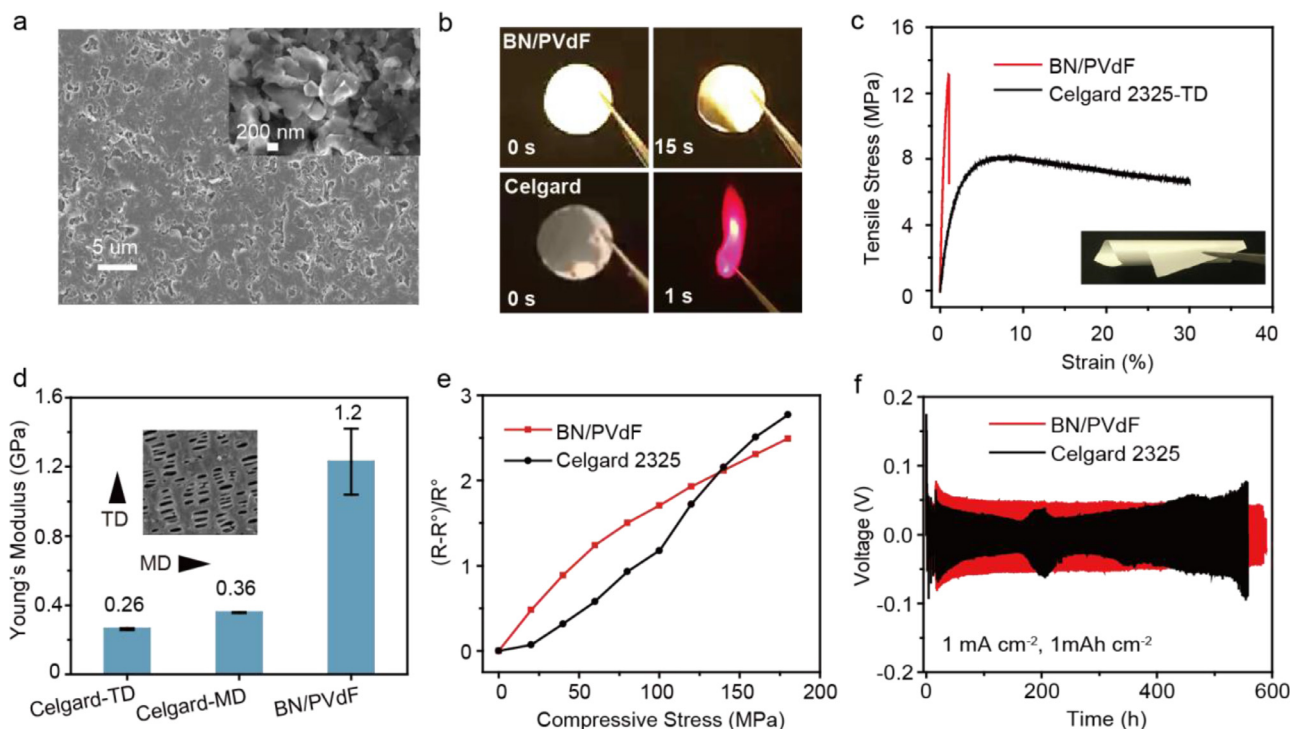


Fig. 3. (a) A SEM image of the as-fabricated BN/PVdF separator with the inset showing the BN nanosheets after sonication. (b) Ignition tests of Celgard 2325 separator and BN/PVdF film wetted by liquid electrolyte (1 M LiTFSI in DOL/DME (v/v, 1:1)). (c) The strain-stress curves of PE separator (Celgard 2325 at transverse direction) and BN/PVdF film with the inset showing the flexible BN/PVdF film. (d) The Young's modulus of a BN/PVdF separator and a PE separator along its machinery direction (MD) and transverse direction (TD). (e) The dependence of resistance upon compressive stress of stainless steel (SS)/separator/SS cells, where the separator is BN/PVdF (red) or commercial (black). (f) The voltage profile of Li/Li symmetric cells at 1.0 mA cm⁻² with the composite BN/PVdF separator (red) or the commercial PE separator (black).

the lithium/OCF is relatively smooth, which confirms the advantage of the carbon fabric skeleton in preventing the growth of lithium dendrite (Fig. S5e–5f).

In addition to introducing the OCF matrix to enhance the tensile strength/Young's modulus of electrode materials, we also developed a BN/PVdF composite to replace the conventional PE separator. As the inorganic filler, BN possesses several desirable attributes including electronic insulation, chemical stability, thermal stability and mechanical robustness [34]. The BN/PVdF composite separator was prepared by sonicating the crumpled-paper-like BN aggregates in a mixed IPA/DMF solvent (Fig. S6a and S6b), followed by connecting the BN nanosheets with PVdF polymer (Fig. 3a). Since BN is nonflammable and PVdF has a flashpoint over 400 °C [35,36], The composite film is far more thermally stable than the PE separator, even with the presence of electrolyte (Supplementary Videos S3 and S4). When ignited, the BN/PVdF separator is difficult to catch fire while the PE separator burns immediately (Fig. 3b). Mechanically, the BN/PVdF film shows higher UTS and modulus (13.1 ± 1.2 MPa and 1.2 ± 0.2 GPa respectively), which are much higher than those of PE separator at the transverse direction (8.0 ± 0.6 MPa and 0.26 ± 0.05 GPa) (Fig. 3c and 3d). In addition to standard mechanical measurements, we also explored how compression affects the ionic conductivity in the two kinds of separators, which helps evaluate the behavior of the batteries under external impact. As shown in Fig. 3e, although the BN/PVdF separator shows higher resistance at intermediate pressure, it outperforms the PE separator with more stable conductivity when the compression exceeds 150 MPa. This result can be attributed to the high-modulus of BN nanofiller that maintains the integrity of the composite separator at extremely high compressive stress. Since the resistance only has a threefold increment under the compression of 180 MPa, it is still acceptable for battery cycling. As shown in Fig. 3f, the Li/Li symmetrical cell with BN/PVdF separator wetted by liquid electrolyte delivers a stable voltage profile over 500 h at 1.0 mA cm⁻²

and 1.0 mA cm⁻², demonstrating excellent lithium plating/stripping reversibility.

After optimizing each component, a structural cell that consists of Li/OCF 400 °C 15 min, BN/PVdF separator and lithium polysulfide on OCF 500 °C 2 h was assembled. For comparison, a regular Li/S cell using lithium foil, celgard 2325 separator and particle-based cathode was also investigated. In terms of electrochemical performance, the structural Li/S cell delivers an initial capacity of 1266 mAh g⁻¹ (sulfur) with the electrolyte-to-sulfur weight ratio of ~27. After a slight drop to 1101 mAh g⁻¹ at the 10th cycle, the capacity stabilizes at 1030 mAh g⁻¹ after 200 cycles (Fig. 4a), which greatly exceeds that of conventional Li/S batteries. As for the rate performance, the discharge capacity for the former reaches 1228, 1069, 923 and 791 mAh g⁻¹ at 0.1, 0.2, 0.5 and 1 C rate respectively, much higher than the latter, which typically delivers discharge capacities of 692, 477, 268 and 60 mAh g⁻¹ at the counterparts (Fig. 4b). The higher discharge capacity along with smaller polarization (Fig. S8a and S8b) confirms the superiority of electrodes with carbon fiber-based structural skeletons. Based on the total mass of battery components, an energy density of 43 Wh kg⁻¹ is estimated for the structural battery (Fig. S7), which exceeds the values in previous reports on structural batteries or supercapacitors (Fig. 4c) [4,9,37–43]. Even when the cell was assembled in pouch configuration, the electrochemical performance of the structural Li/S cell is still significantly superior to the regular one (Fig. S8d). It should be noted that the amount of electrolyte needs to be significantly reduced for practical applications (< 3 g Ah⁻¹) [44,45]. Great efforts will be needed to realize practical structural Li/S battery in the future.

Besides testing in ambient conditions, we also investigate the cells under abused conditions. Fig. 4d and Fig. S8a–8b shows the electrochemical performance of the two batteries at different compressive stress (up to 20 MPa). The structural battery exhibits a discharge capacity of 1093 mAh g⁻¹ when compressive stress of 10 MPa is applied, much higher

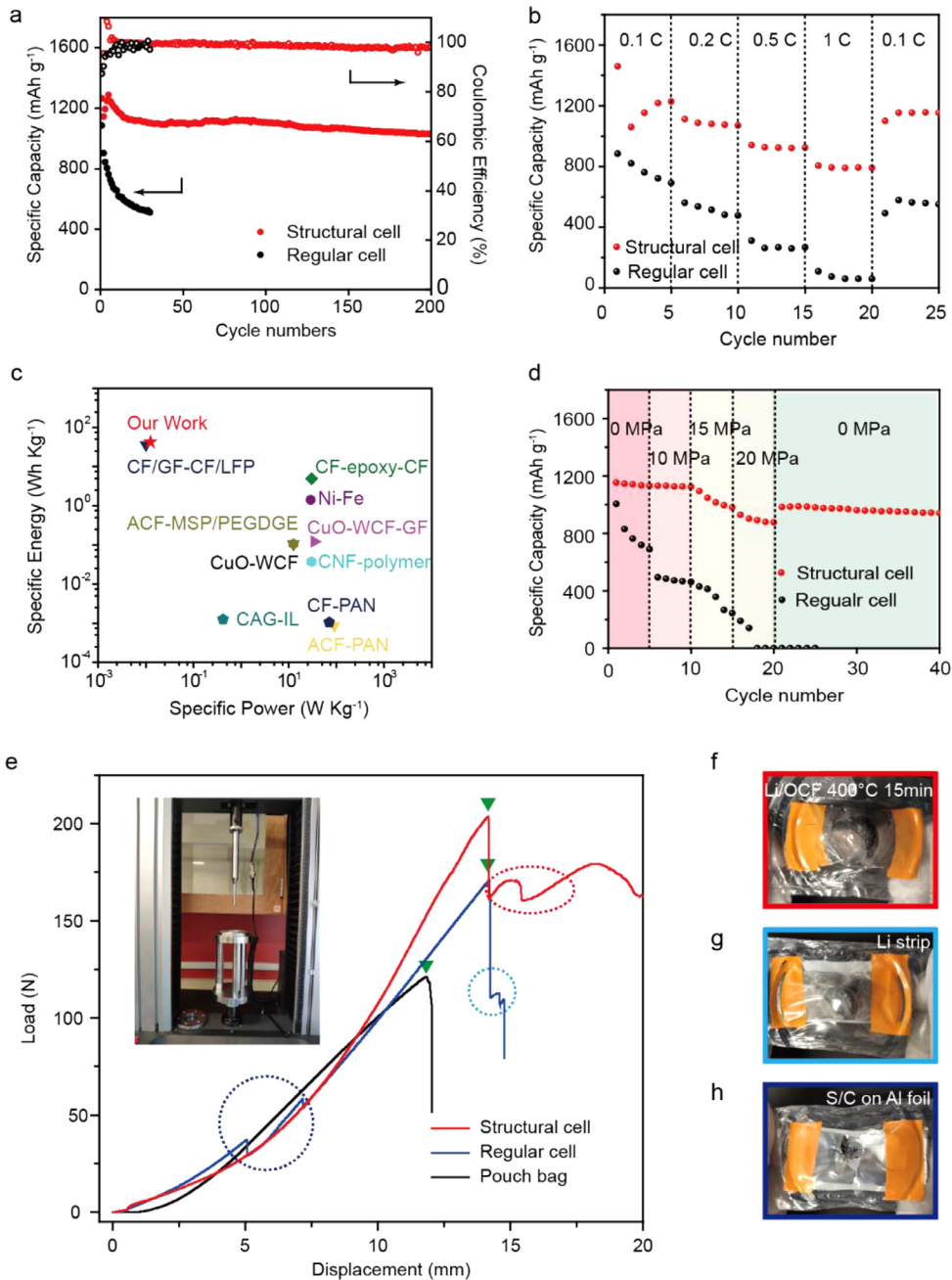


Fig. 4. The comparison of cycling performance of the optimized structural cell and the regular cell at (a) 0.2 C and (b) different C-rates. The sulfur loading is $\sim 1.0 \text{ mg cm}^{-2}$. (c) The Ragone diagram for the energy and power density based on the sulfur loading of 2.3 mg cm^{-2} and the total mass of the whole components compared to other state-of-the-art structural energy storage devices in literatures. (d) The electrochemical performance of the two cells at various compressive stresses. (e) The load-displacement diagrams for the two cells in pouch cell configurations. The inset shows the test assembly used for the static puncture tests. The fracture was reflected from peaks in the curves (marked with colorful circles) of (f) Li/OCF $400 \text{ }^\circ\text{C}$ 15 min (red), (g) Li foil (blue), (h) S/C on aluminum foil (navy). The peak (marked with green triangles) at the top of each curve represents the destruction of the transparent pouch bag.

than 429 mAh g^{-1} of the regular cell. Even when the stress increases to 20 MPa, it still remains 981 mAh g^{-1} for the structural cell. In contrast, the regular Li/S cell fails with the capacity decaying to almost zero. The difference might originate from the distinct anodes. The creep-induced metallic lithium would penetrate into the pores of the PE separator at such overloaded pressure (20 MPa), thereby creating an electric percolation pathway that shorts the cell internally, which can be confirmed by the severe deformation of the anode in Fig. S8c and corresponds to recent reports [46,47]. In contrast, benefiting from high Young's modulus, the shape of the Li/OCF was almost consistent with their initial state. This result demonstrates that the electrode enhanced with carbon fabrics possesses excellent resistance to mechanical stress. After removal of the external stress, the capacity in structural cell recovers to 983 mAh g^{-1} . In contrast, no capacity was left for the conventional Li/S cell, and the voltage profile indicates that the cell's internal resistance increased remarkably, which can be attributed to the cracks

of the electrode and the closure of pores in the separator under high pressure (Fig. S8c). Furthermore, the good mechanical property for the structural Li/S cell is confirmed by a puncture test, which is a harsh risk assessment including both tensile and compressive stresses. From the results, the peak at the top of each curve (marked with green triangles) represents the fracture of the transparent pouch bag. It is also found that no breaks appeared for the structural cathode and the flat woven CF was only stretched by the slim probe (Fig. S9). Therefore, the maximum tolerance for the cathode should exceed 204 N. Accordingly, the fractures of other electrodes were assigned and marked with the same colorful circles, respectively. It can be judged from Fig. 4f-4h that the structural electrodes were destroyed at higher puncture loads when compared to the regular cell ($>204 \text{ N}$ vs. 50 N for the cathodes, and 170 N vs 110 N for the anodes), which suggests that the introduction of carbon fabrics skeleton can effectively withstand the harsh mechanical deformation.

3. Conclusion

In summary, we have successfully verified that the feasibility for improving the mechanical strength of structural batteries via conformally-coated electrodes. As a prototype, the Li/S battery system was introduced into the field of structural batteries for the first time. Both electrodes were prepared by electrodeposition-like reactions, together with the carbon fabric skeleton to endow them with mechanical robustness. The as-obtained structural Li/S cell displays good tolerance to mechanical deformation such as compression and puncture tests. Additionally, the new BN/PVdF separator, specifically for the structural Li/S cell effectively enhanced its compressive capability. The battery can cycle for 20 times stably under a pressure up to 20 MPa. Moreover, the energy density of the structural battery based on the total mass reached 43 Wh kg⁻¹. This work provides a promising strategy to build a multifunctional structural energy storage platform so as to enhance the mechanical strength and energy density for structural batteries.

4. Experimental section

4.1. Materials

Commercial PAN-based CF (T300, thickness of 200 μm) was bought from FibreGlast Development Corp. Boron nitride (BN) micropowder was purchased from Graphene Supermarket, Inc. Lithium bis (trifluoromethane sulfonyl) imide (LiTFSI) was obtained from Gotion, Inc. Polyvinylidene fluoride binder (PVdF 761) was received from Arkema Inc. Microporous polyolefin membrane (Celgard 2325, 25 μm thickness, PE/PP/PE trilayer) was obtained from Celgard, LLC and used for comparison. Lithium strip (99.9%, thickness of 0.75 mm) for mechanical tests and Lithium sulfide (Li₂S, 99.9%) were purchased from Alfa Aesar. All the other reagents and solvents were obtained from Sigma-Aldrich and used as received.

4.2. Fabrication of structural Li/S battery

4.2.1. Electrode fabrication

Commercial T300 CF was first heated in air at different temperatures to remove the sizing agent on the surface, which is denoted as OCF. For the cathode, the OCF is combined with 1 M Li₂S₈, 0.5 M LiTFSI and 1 wt% LiNO₃ in DOL/DME. For the anode, the treated CF was immersed into molten lithium until the metal was fully absorbed. The as-obtained lithium/OCF was scraped to make the surface flat and then cut into appropriate shapes. Before use, the lithium/OCF was pretreated in 0.5 M LiTFSI in DOL/DME solution with 1 wt% LiNO₃ additive for 1.5 hours so as to form a passivation layer [48].

4.2.2. Preparation of the BN/PVdF separator

Porous BN/PVdF composite film was fabricated via the phase-inversion method as follows. The BN powder (200.0 mg) was added into mixed IPA/DMF (12.0 g/1.25 g) solvents and well dispersed via a sonicator (FE 110D, Fisher Scientific) for 48 h, following which the homogeneous suspension was stirred vigorously at 100 °C to remove IPA. The PVdF761 (100.0 mg) and LiTFSI (75.0 mg) were then added to the slurry with stirring for 2.5 h continuously at 70 °C. The weight ratio of BN to PVdF is 2:1 in this paper unless other ratios are mentioned. The slurry was blade-coated onto a clean glass plate and dried at 60 °C for 0.5 h. The BN/PVdF film is peeled off from the glass plate after immersed it into DI water. The added LiTFSI will be dissolved into the water and make pores for the lithium ion passage. Then the film is dried to remove residual water.

4.2.3. Cell fabrication

The as-prepared structural cathode, structural anode (~250 μm) and BN/PVdF separator (~50 μm) are combined together in 2032-coin cells for electrochemical and mechanical tests. The electrolyte is 1.0 mol

L⁻¹ LiTFSI with 2.0 wt% anhydrous LiNO₃ as the additive in a mixed dimethoxyethane (DME) and 1, 3-dioxolane (DOL) (V: V=1:1) solvents. The amount of liquid electrolyte that wets the BN/PVdF separator is 20 μL.

4.3. Preparation of the conventional Li/S battery

The regular sulfur cathode was prepared by mixing 60 wt% sulfur, 30 wt% carbon black and 10 wt% PVdF in N-methyl-2-pyrrolidone (NMP) solvent to form a homogeneous slurry. The slurry was then cast onto aluminum foil and dried at 60 °C under vacuum for 8 h. The mass loading is ~1 mg cm⁻². Then it is combined with conventional PE separator and 250 μm-thick lithium anode and assembled in a 2032-coin cell. The lithium anode was pretreated in the same condition above to obtain a passivation layer. The liquid electrolyte used was the same as that in the structural battery.

4.4. Electrochemical measurements

The galvanostatic charge-discharge tests were performed using a battery test system (C2001A, LAND, China) with the cutoff voltage between 1.7–2.8 V. The ionic conductivity of porous BN/PVdF was measured by testing the AC impedance of its stainless-steel symmetrical cells. The frequency ranges from 1 M Hz to 1 Hz. The ionic conductivity was calculated by the equation $\sigma = L/RS$, where R was the bulk resistance, L and S were the thickness and the area of the BN/PVdF film, respectively.

4.5. Material characterization

The morphology of the structural electrodes was acquired via a scanning electron microscope (Zeiss SIGMA VP). The surface analyses of OCFs were performed by a PHI 5500XPS with a monochromatic Al K α X-ray excitation source (1486.6 eV).

4.6. Mechanical measurements

The bending tests were conducted to verify the designed battery available for maintaining mechanical robustness. Lithium cobalt oxide (LCO) on aluminum foil was taken as an example for the particle-based planar electrode while lithium polysulfide in DOL/DME was loaded onto the OCF 500 °C 2 h as the electrodeposition-like electrode. For the LCO electrode, the slurry consists of 92 wt% LCO, 5 wt% C65, 3 wt% PVdF761 with N-methyl-2-pyrrolidone (NMP) as the solvent. The LCO and polysulfides cathode has the same areal capacity (~4 mAh cm⁻²) on planar aluminum foil or carbon fabrics, which corresponds to different cathodes in Fig. 1a-1c, respectively. All the cathodes are bent back and forth over 200 times (Servo motor programmable controller KH-01, China) with moderate frequency (also see the Supplementary Video S1). It should be noted that a transparent pouch bag was used to seal the LiPS/OCF cathode so as to prevent the leakage of toxic gas when exposed to air during the test.

To perform tensile measurements, CF was cut into long strips with the size about 1 inch × 2.5 inch in length and then epoxy resin and stainless steel were used to make tabs enabling gripping the structural materials. Tensile tests for the CF-based electrodes were conducted using an Instron load cell at a strain rate of 2 × 10⁻⁴ s⁻¹. All the results are obtained on the basis of testing three samples. *In-situ* mechano-electrochemical measurements were performed on Instron tester (model 1321) with a portable Bio-logic VMP3 potentiostat to record the electrochemical performance synchronal.

To investigate the mechanical stability of pouch cells, puncture tests were conducted to determine their puncture or rupture characteristics. This is both a compressive and tensile test where a cell is compressed by a 7 mm diameter steel probe at a speed of 5 mm min⁻¹ until the material ruptures. The mechanical failure of the structural electrodes is reflected by the sharp peaks and the force-displacement curves were recorded.

Author contributions

W.H. and P.W. contributed equally to this work. Y.Y. and W.H. conceived and designed the experiments. W.H. and P.W. carried out materials synthesis, electrochemical and mechanical characterizations. X.L., Y.C., J.B., Q.C., H.Z. and Z.S. provided helpful suggestions for this work. T.J., A.L., Y.Z. and A.C. assisted with the mechanical characterizations. W.H., P.W. and Y.Y. wrote the paper together. All authors discussed the results and commented on the manuscript.

Declaration of Competing Interest

The authors declare that they have no known competing financial interests or personal relationships that could have appeared to influence the work reported in this paper.

Acknowledgments

Y. Yang acknowledges support from Air Force Office of Scientific Research (FA9550-18-1-0410 and FA9550-20-1-0233). W. Huang would like to acknowledge the financial support from the China Scholarship Council (No. 201806250099).

Supplementary materials

Supplementary material associated with this article can be found, in the online version, at doi:10.1016/j.ensm.2020.08.018.

References

- [1] H.C. Kim, T.J. Wallington, *Environ. Sci. Technol.* 47 (2013) 6089–6097.
- [2] D. R. Tenney, E. A. Starke Jr, J. C. Newman Jr, J. Heyman and T. T. Bales, (2019).
- [3] P. Flouda, X.Y. Feng, J.G. Boyd, E.L. Thomas, D.C. Lagoudas, J.L. Lutkenhaus, *Batteries & Supercaps* 2 (2019) 464–472.
- [4] E. Senokos, Y. Ou, J.J. Torres, F. Sket, C. González, R. Marcilla, J.J. Vilatela, *Sci. Rep.* 8 (2018) 3407.
- [5] J. Silva-Leon, A. Gioncolini, M.R. Nabawy, A. Revell, A. Kennaugh, *Appl. Energy* 239 (2019) 846–858.
- [6] K. Shanks, J.P. Ferrer-Rodriguez, E.F. Fernández, F. Almonacid, P. Pérez-Higueras, S. Senthilarasu, T. Mallick, *Sol. Energy* 169 (2018) 457–467.
- [7] S.R. Kwon, J. Harris, T. Zhou, D. Loufakis, J.G. Boyd, J.L. Lutkenhaus, *ACS Nano* 11 (2017) 6682–6690.
- [8] S. on Tung, S.L. Fisher, N.A. Kotov, L.T. Thompson, *Nat. Commun.* 9 (2018) 4193.
- [9] K. Moyer, C. Meng, B. Marshall, O. Assal, J. Eaves, D. Perez, R. Karkkainen, L. Roberston, C.L. Pint, *Energy Stor. Mater.* 24 (2020) 676–681.
- [10] L.E. Asp, E.S. Greenhalgh, *Compos. Sci. Technol.* 101 (2014) 41–61.
- [11] J. F. Snyder, D. J. O'Brien, D. M. Baechle, D. E. Mattson and E. D. Wetzel, *Structural composite capacitors, supercapacitors, and batteries for US Army Applications* (2008).
- [12] E. D. Wetzel, D. J. O'Brien, J. F. Snyder, R. H. Carter and J. T. South, *Multifunctional structural power and energy composites for US army applications, ARMY RESEARCH LAB ABERDEEN PROVING GROUND MD WEAPONS AND MATERIALS RESEARCH DIRECTORATE* (2006).
- [13] J.F. Snyder, R.H. Carter, E.D. Wetzel, *Chem. Mater.* 19 (2007) 3793–3801.
- [14] T. Carlson, D. Ordeus, M. Wysocki, L.E. Asp, *Compos. Sci. Technol.* 70 (2010) 1135–1140.
- [15] N. Muralidharan, E. Teblum, A.S. Westover, D. Schauben, A. Itzhak, M. Muallem, G.D. Nessim, C.L. Pint, *Sci. Rep.* 8 (2018) 17662.
- [16] P. Flouda, S.A. Shah, D.C. Lagoudas, M.J. Green, J.L. Lutkenhaus, *Matter* (2019).
- [17] W. Johannisson, N. Ihrner, D. Zenkert, M. Johansson, D. Carlstedt, L.E. Asp, F. Sieland, *Compos. Sci. Technol.* 168 (2018) 81–87.
- [18] C. Meng, N. Muralidharan, E. Teblum, K.E. Moyer, G.D. Nessim, C.L. Pint, *Nano Lett.* 18 (2018) 7761–7768.
- [19] L.E. Asp, E.S.J.C.s. Greenhalgh, and technology 101 (2014) 41–61.
- [20] E. Wong, D. Baechle, K. Xu, R. Carter, J. Snyder, E. Wetzel, *Design and processing of structural composite batteries, ARMY RESEARCH LAB ABERDEEN PROVING GROUND MD*, 2007.
- [21] R. Xu, J. Yue, S. Liu, J. Tu, F. Han, P. Liu, C. Wang, *ACS Energy Lett.* 4 (2019) 1073–1079.
- [22] H. Li, S. Wang, M. Feng, J. Yang, B. Zhang, J. Mater. Sci. 53 (2018) 11607–11619.
- [23] D. Carlstedt, E. Marklund, L.E. Asp, *Compos. Sci. Technol.* 169 (2019) 26–33.
- [24] Y. Chen, S. Choi, D. Su, X. Gao, G. Wang, *Nano Energy* 47 (2018) 331–339.
- [25] Y. Chen, W. Zhang, D. Zhou, H. Tian, D. Su, C. Wang, D. Stockdale, F. Kang, B. Li, G. Wang, *ACS Nano* 13 (2019) 4731–4741.
- [26] J.F. Snyder, E.D. Wetzel, C.M. Watson, *Polymer* 50 (2009) 4906–4916.
- [27] J.F. Snyder, E.B. Gienger, E.D. Wetzel, *J. Compos. Mater.* 49 (2015) 1835–1848.
- [28] H. Chu, H. Noh, Y.-J. Kim, S. Yuk, J.-H. Lee, J. Lee, H. Kwack, Y. Kim, D.-K. Yang, H.-T. Kim, *Nat. Commun.* 10 (2019) 188.
- [29] Z. Wang, J. Shen, J. Liu, X. Xu, Z. Liu, R. Hu, L. Yang, Y. Feng, J. Liu, Z. Shi, L. Ouyang, Y. Yu, M. Zhu, *Adv. Mater.* 31 (2019) 1902228.
- [30] J. Song, X. Guo, J. Zhang, Y. Chen, C. Zhang, L. Luo, F. Wang, G. Wang, *J. Mater. Chem. A* 7 (2019) 6507–6513.
- [31] D.C. Lin, Y.Y. Liu, Z. Liang, H.W. Lee, J. Sun, H.T. Wang, K. Yan, J. Xie, Y. Cui, *Nat. Nanotechnol.* 11 (2016) 626–632.
- [32] W. Go, M.H. Kim, J. Park, C.H. Lim, S.H. Joo, Y. Kim, H.W. Lee, *Nano Lett.* 19 (2019) 1504–1511.
- [33] J.H. Kim, Y.H. Lee, S.J. Cho, J.G. Gwon, H.J. Cho, M. Jang, S.Y. Lee, S.Y. Lee, *Energy Environ. Sci.* 12 (2019) 177–186.
- [34] W. Luo, L. Zhou, Z. Yang, J. Dai, E. Hitz, Y. Kuang, X. Han, B. Yang, L. Hu, *Nano Energy* 40 (2017) 149–154.
- [35] W. Luo, L. Zhou, K. Fu, Z. Yang, J. Wan, M. Manno, Y. Yao, H. Zhu, B. Yang, L. Hu, *Nano Lett.* 15 (2015) 6149–6154.
- [36] P. Yao, B. Zhu, H. Zhai, X. Liao, Y. Zhu, W. Xu, Q. Cheng, C. Jayyosi, Z. Li, J. Zhu, K.M. Myers, X. Chen, Y. Yang, *Nano Lett.* 18 (2018) 6113–6120.
- [37] H. Qian, A.R. Kucernak, E.S. Greenhalgh, A. Bismarck, M.S. Shaffer, *ACS Appl. Mater. Interfaces* 5 (2013) 6113–6122.
- [38] N. Shirshova, H. Qian, M.S.P. Shaffer, J.H.G. Steinke, E.S. Greenhalgh, P.T. Curtis, A. Kucernak, A. Bismarck, *Compos. Part A Appl. Sci. Manuf.* 46 (2013) 96–107.
- [39] B.K. Deka, A. Hazarika, J. Kim, Y.-B. Park, H.W. Park, *Compos. Part A Appl. Sci. Manuf.* 87 (2016) 256–262.
- [40] Y. Wang, X. Qiao, C. Zhang, X. Zhou, *ECS Trans.* 72 (2016) 31–44.
- [41] K.-Y. Chan, B. Jia, H. Lin, N. Hameed, J.-H. Lee, K.-T. Lau, *Compos. Struct.* 188 (2018) 126–142.
- [42] A. Javadi, K.K.C. Ho, A. Bismarck, J.H.G. Steinke, M.S.P. Shaffer, E.S. Greenhalgh, *J. Compos. Mater.* 52 (2018) 3085–3097.
- [43] C. Meng, N. Muralidharan, E. Teblum, K.E. Moyer, G.D. Nessim, C.L. Pint, *Nano Lett.* 18 (2018) 7761–7768.
- [44] W. Xue, Z. Shi, L. Suo, C. Wang, Z. Wang, H. Wang, K.P. So, A. Maurano, D. Yu, Y. Chen, L. Qie, Z. Zhu, G. Xu, J. Kong, J. Li, *Nat. Energy* 4 (2019) 374–382.
- [45] C. Niu, H. Pan, W. Xu, J. Xiao, J.-G. Zhang, L. Luo, C. Wang, D. Mei, J. Meng, X. Wang, Z. Liu, L. Mai, J. Liu, *Nat. Nanotechnol.* 14 (2019) 594–601.
- [46] J.-M. Doux, H. Nguyen, D.H.S. Tan, A. Banerjee, X. Wang, E.A. Wu, C. Jo, H. Yang, Y.S. Meng, *Adv. Energy Mater.* 10 (2020) 1903253.
- [47] J.-M. Doux, Y. Yang, D.H.S. Tan, H. Nguyen, E.A. Wu, X. Wang, A. Banerjee, Y.S. Meng, *J. Mater. Chem. A* 8 (2020) 5049–5055.
- [48] Y. Yang, G.Y. Zheng, Y. Cui, *Energy Environ. Sci.* 6 (2013) 1552–1558.